Articles

Analysis of a Water Mediated Protein−Protein Interactions within RNase T1[†,‡]

Ulrike Langhorst, Jan Backmann, Remy Loris, and Jan Steyaert*

Dienst Ultrastructuur, Vlaams Interuniversitair Instituut Biotechnologie, Vrije Universiteit Brussel, Paardenstraat 65, B-1640 Sint-Genesius-Rode, Belgium

Received September 13, 1999; Revised Manuscript Received March 13, 2000

ABSTRACT: Buried and well-ordered solvent molecules are an integral part of each folded protein. For a few individual water molecules, the exchange kinetics with solvent have been described in great detail. So far, little is known about the energetics of this exchange process. Here, we present an experimental approach to investigate water-mediated intramolecular protein−protein interactions by use of double mutant cycles. As a first example, we analyzed the interdependence of the contribution of two side chains (Asn9 and Thr93) to the conformational stability of RNase T1. In the folded state, both side chains are involved in the "solvation" of the same water molecule WAT1. The coupling of the contributions of Asn9 and Thr93 to the conformational stability of RNase T1 was measured by urea unfolding and differential scanning calorimetry. The structural integrity of each mutant was analyzed by X-ray crystallography. We find that the effects of the Asn9Ala and the Thr93Ala mutations on the conformational stability are additive in the corresponding double mutant. We conclude that the free energy of the WAT1 mediated intramolecular protein−protein interaction in the folded state is very similar to solvent mediated protein−protein interaction in the unfolded state.

Water molecules are an integral part of the folded state of a protein. In a number of cases, water molecules have been found to be conserved among homologous proteins (*1*−*3*), suggesting that they are structurally or functionally important. Solvent molecules can be buried deep inside the globular protein or located in crevices near the surface (*4*). A small number of well-defined water molecules at internal cavities have residence times in the range from 10^{-2} to 10^{-8} s (*5*, *6*). The remaining molecules, although some are well-defined in the X-ray structure, have subnanosecond residence times, similar to those waters that are exposed on the surface of the protein.

The number of hydrogen bonds formed between these water molecules and the protein varies from 0 to 4, with 3 being most common (*7*). The geometry of the network is generally approximately tetrahedral; the hydrogen bond lengths are close to optimal (∼2.8 Å) (*8*). From a set of 75 high resolution, nonhomologous monomeric protein structures, the likelihood of a cavity being hydrated or not has been analyzed in function of the number of potential polar contacts to a water placed at the center. This statistical approach indicates that a buried water−protein hydrogen bond stabilizes the folded protein by ±0.6 kcal/mol (*7*).

Recently, we investigated the structural and functional features of a conserved hydration site in a crevice near the surface of RNase T1 (*9*). Figure 1a presents the geometry around this hydration site. Structurally, the closest hydrogen bond donor/acceptor sites Cys6(O), Asp76(Oδ1), and Thr93(Oγ1) occupy three corners of an almost perfect tetrahedron with WAT1 in the center. WAT1 is, however, not rigidly fixed in this site and alternative hydrogen-bonding schemes involving Asn9(Nδ2) and Thr91(Oγ1) can be envisaged. Although this solvent molecule is well ordered in the X-ray structure, it exchanges with the solvent in the nanosecond range (*9*). Here, we examine the contributions of Asn9 and Thr93 to the conformational stability of RNase T1 by double-mutant cycle analysis to evaluate the energetics of the water-mediated intramolecular protein−protein interactions of this hydration site.

MATERIALS AND METHODS

Oligonucleotide-Directed Mutagenesis and Purification of RNase T1. Overproduction and purification of wild-type RNase T1 have been described previously (*10*). The Asn9Ala, Thr93Ala, and Asn9Ala/Thr93Ala mutants were constructed with a PCR-based[1] site-directed mutagenesis technique (*11*).

[†] This work was supported by the Vlaams Interuniversitair Instituut voor Biotechnologie (VIB) and the Fonds voor Wetenschappelijk Onderzoek (FWO) Vlaanderen.

[‡] Refined coordinates and structure factors have been deposited in the Brookhaven Protein Data Bank: PDB ID codes 1BVI, 2HOH, 4HOH, 5HOH.

* Corresponding Author: Jan Steyaert, Dienst Ultrastructuur, Vlaams Interuniversitair Instituut Biotechnologie, Vrije Universiteit Brussel, Paardenstraat 65, B-1640 Sint-Genesius-Rode. Tel: +/32/2/359 02 48. Fax: +/32/2/359 02 89. Email: jsteyaer@vub.ac.be.

[1] Abbreviations: DSC, differential scanning calorimetry; $\Delta G(H_2O)$, free energy in absence of denaturant; m, $\delta\Delta G/\delta$[urea]; ΔH_{vH}, van't Hoff enthalpy; ΔH_{trs}, calorimetric enthalpy of unfolding at transition temperature; T_{trs}, temperature at which the fraction of unfolded protein

10.1021/bi992131m CCC: $19.00
Published on Web 05/12/2000

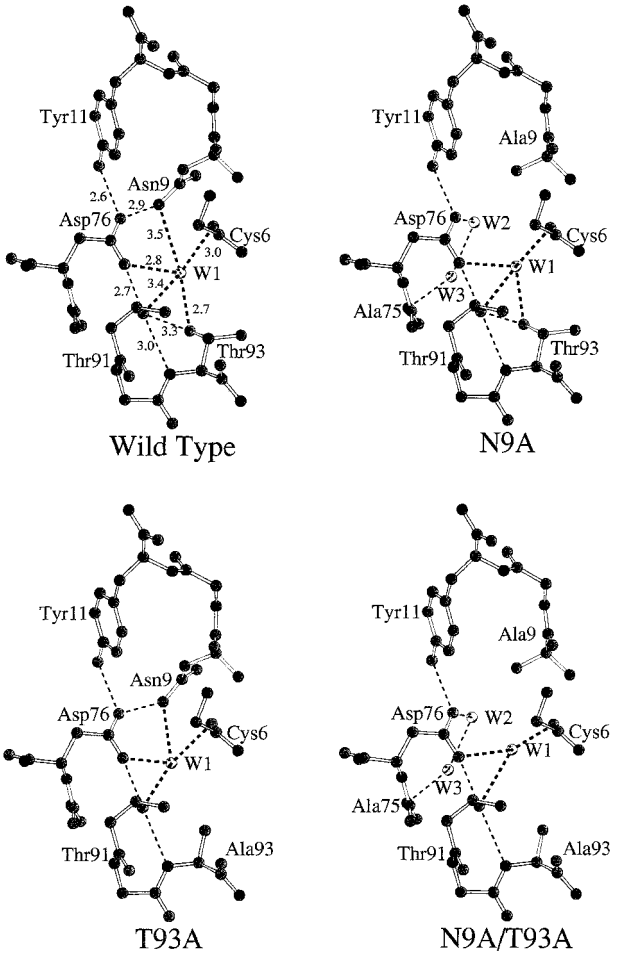

FIGURE 1: Comparison of the local hydrogen bond networks around WAT1 in wild-type Rnase T1 and the three mutants of the double mutant cycle. In each case, molecule A is shown. The local structures of the other three molecules (B, C, and D) in the asymmetric unit of the crystal are essentially identical. (a) wild-type, all relevant interatomic distances are shown; (b) Asn9Ala; (c) Thr93Ala; (d) Asn9Ala/Thr93Ala.

The correct sequence of the complete gene was verified by DNA sequencing. Enzymes were purified to homogeneity as described (*12*) and their molecular weights were confirmed by mass spectrometry (data not shown).

Crystal Structure Determination. We obtained isomorphous crystals of wild-type, Asn9Ala, Thr93Ala, and Asn9Ala/Thr93Ala RNase T1 in complex with the specific inhibitor 2′-GMP using the sitting drop technique aided by macroseeding (see Table 1 for all details). Data were collected using a MAR Image Plate detector and a RIGAKU Rotating anode X-ray generator operated at 40 kV, 90 mA. The data were integrated using DENZO and subsequently scaled and merged using SCALEPACK (*13*). The CCP4 program TRUNCATE (*14*) was used to convert I's into F's. The statistics of the data collections are summarized in Table 1.

The structure of the Thr93Ala mutant was solved by molecular replacement with the program AMORE (*15*) using PDB entry 1rga (*16*). For the other mutants as well as wild-type RNase T1, the refined structure of the Thr93Ala mutant was used as the starting model for refinement. All refinements were done with X-PLOR version 3.851 (*17*) using all measured reflections. A bulk solvent correction was calculated after each rebuilding session. In each structure, five copies of the inhibitor 2′GMP and two calcium ions were identified in the electron density map. Water molecules were included (1) if they could be identified as peaks of at least 3σ in $F_o - F_c$ maps, (2) if they reappeared after refinement in $2F_o - F_c$ maps of at least 1σ, (3) if they made at least one reasonable hydrogen bond to a protein or inhibitor atom, and (4) if they showed no van der Waals clashes with any protein or inhibitor atom or with a previously identified water molecule. The quality of all refined structures was verified with PROCHECK (*18*) and is described in Table 1.

Urea Unfolding. Urea denaturation experiments were performed according to Pace (*19*). Protein concentration were determined by UV absorbance using $A_{278nm} = 1.74$ for a 0.1% solution (*20*). Unfolding of RNase T1 was measured by following the fluorescence decrease at 320 nm upon excitation at 278 nm with an Aminco-500 fluorimeter. Samples of RNase T1 (20 μg/mL) were incubated overnight in 30 mM MOPS buffer, pH 7.0, to reach equilibrium at 15, 25, or 35 °C. The urea concentration was controlled by refractive index measurements. Urea denaturation curves were processed by applying a linear extrapolation method (LEM) based fitting function described in Santoro and Bolen (*21*). The pre- and posttransitional baseline of the urea unfolding curves at 15 and 35 °C, respectively, are too short for accurate analysis of the *m* value by LEM. At these temperatures, we determined the [$urea_{1/2}$]-point accurately and calculated $\Delta G(H_2O)$ according to $m\cdot[urea_{1/2}]$ using an average $m = 1247 \pm 0.025$ kcal (mol M)$^{-1}$ obtained from all measurements at 25 °C.

Differential Scanning Calorimetry. Scanning calorimetric measurements were performed on a MicroCal MC-2 scanning calorimeter. Protein solutions were prepared by dissolving salt-free, freeze-dried protein powder in buffer. The solution was then loaded on a PD-10 column (Pharmacia Biotech AB) packed with Sephadex G-25 and eluted with the same buffer to equilibrate solution conditions. The concentration was determined as described above. Protein solutions were degassed by stirring them 5 min under vacuum. The buffers were 30 mM NaAc at pH 5.0, 30 mM Mops at pH 7.0, and 30 mM Glycine/NaOH at pH 10.0. Thermograms were obtained at a scan rate of 60 °C/min. For each sample, two consecutive scans were executed to monitor the reversibility of the protein unfolding. From each protein, two experiments were carried out and the results averaged. The obtained thermograms were processed with the MicroCal ORIGIN software to obtain the calorimetric molar enthalpy of unfolding at transition temperature ΔH_{trs}, the van't Hoff enthalpy ΔH_{vH} and the transition temperature T_{trs}.

Data Analysis. Assuming that ΔC_p does not depend on temperature in the regarded temperature range, the dependence of the Gibbs' free-energy change $\Delta G(H_2O)$ on temperature is given by a modified Gibbs−Helmholtz equation:

equals $^1/_2$; ΔC_p, change in heat capacity upon unfolding; PCR, polymerase-chain-reaction; 2′-GMP, 2′-guanylic acid, NaAc, sodium acetate; Mops, 3-(*N*-morpholino)propanesulfonic acid; MPD, 2-methyl-2,4-pentanediol.

$$\Delta G(T) = \Delta H_{trs}\left(\frac{T_{trs} - T}{T_{trs}}\right) - \Delta C_p(T_{trs} - T) + T\Delta C_p \ln\left(\frac{T_{trs}}{T}\right) \quad (1)$$

where T_{trs} is the transition temperature, ΔH_{trs} the calorimetric determined enthalpy of unfolding at T_{trs}, and ΔC_p is the change in heat capacity upon unfolding. The equation was used to correlate the results of the urea- and temperature-induced unfolding experiments. Equation 1 was obtained combining $\Delta G = \Delta H - T\Delta S$ with

$$\Delta H(T) = \Delta H_{trs} - \Delta C_p(T_{trs} - T) \quad (2)$$

$$\Delta S(T) = \frac{\Delta H_{trs}}{T_{trs}} - \Delta C_p \ln\left(\frac{T_{trs}}{T}\right) \quad (3)$$

RESULTS AND DISCUSSION

Double Mutant Cycles To Evaluate Protein−Water Interactions. Double-mutant cycles have been used extensively to measure the strength of intramolecular and intermolecular interactions in proteins or protein−ligand complexes (*22*). Additivity of the effects of individual mutations in the corresponding double mutants breaks down where the mutated residues interact with each other, by direct contact or indirectly through electrostatic interactions or structural perturbations, so that they no longer behave independently (*23*).

To analyze the interactions between Asn9, Thr93, and WAT1 in all its details, one should ideally be able to remove WAT1 in the wild-type protein and the mutants to extend the described double mutant cycle to a "triple mutant" box

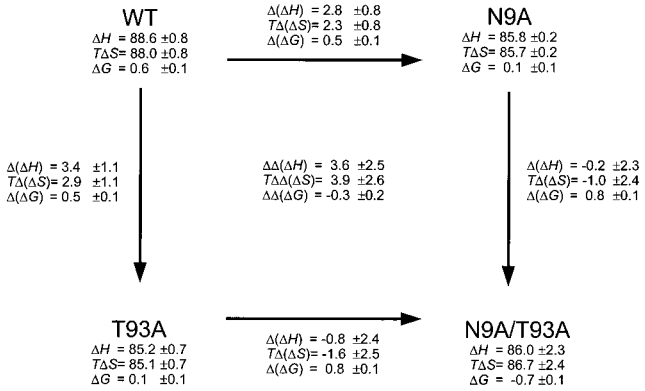

FIGURE 2: Triple mutant box to analyze the interactions between Asn9, Thr93, and WAT1.

(Figure 2). The front cycle of this box measures the strength of the water-mediated mutual interactions between Asn9 and Thr93 (see below). The back cycle measures the water-independent mutual interactions between Asn9 and Thr93. The top and bottom cycles measure the interactions between WAT1 and Asn9 in the presence and absence of the Thr93 side chain, respectively. The left and right cycles probe the interactions between the side chain of Thr93 and WAT1 in the presence (left) or the absence (right) of Asn9. Unfortunately, the controlled elimination of individual water molecules from a protein without disturbing its structure is presently technically impossible. One option would be to replace waters with side chains by protein engineering (*6*, *9*) by xenon or krypton (*24*) or by small ligands (*25*, *26*) and to evaluate the thermodynamics of these substitutions by double mutant cycles.

Table 1: Crystallographic Data

	wild-type	Asn9Ala	Thr93Ala	Asn9Ala/Thr93Ala
PDB ID code	1BVI	2HOH	4HOH	5HOH
crystallization conditions	10 mg/mL protein 25 mM NaAc, pH 4.2 2.8 mM 2′GMP 6.25 mM $CaCl_2$ 47.5% MPD[a]	10 mg/mL protein 25 mM NaAc, pH 4.2 2.8 mM 2′GMP 6.25 mM $CaCl_2$ 45.0% MPD[a]	10 mg/mL protein 25 mM NaAc, pH 4.2 2.8 mM 2′GMP 6.25 mM $CaCl_2$ 42.5% MPD[a]	10 mg/mL protein 25 mM NaAc, pH 4.2 2.8 mM 2′GMP 6.25 mM $CaCl_2$ 40.0% MPD[a]
space group	$P2_12_12_1$	$P2_12_12_1$	$P2_12_12_1$	$P2_12_12_1$
unit cell				
a (Å)	59.34	59.37	59.32	59.35
b (Å)	60.59	60.56	60.31	60.51
c (Å)	100.93	101.17	101.03	101.15
no. of molecules per asymmetric unit	4	4	4	4
no. of unique reflections	28 421	28 731	21 739	25 314
no. of measured reflections	138 761	205 057	64 065	183 837
completeness	96.7%	98.0%	92.8%	100%
resolution (Å)	20.0−1.90	15.0−1.90	15.0−2.05	50.0−2.00
R_{merge}	0.061	0.124	0.065	0.108
$I/\sigma I$	15.9	13.3	11.9	14.3
R-value	0.177	0.168	0.190	0.166
R_{free}-value	0.219	0.209	0.234	0.212
Ramachandran				
most favored (%)	91.0	91.6	90.7	91.0
additionally allowed (%)	8.7	8.1	9.0	8.7
generous (%)	0.3	0.3	0.3	0.3
disallowed (%)	0.0	0.0	0.0	0.0
RMS				
bond lengths (Å)	0.006	0.006	0.007	0.007
bond angles (deg)	1.469	1.265	1.452	1.482
dihedral angles (deg)	24.653	25.183	24.820	24.964
improper angles (deg)	1.037	1.019	1.067	1.067
no. of water molecules per asymmetric unit	242	212	219	215

[a] MPD, 2-methyl-2,4-pentanediol.

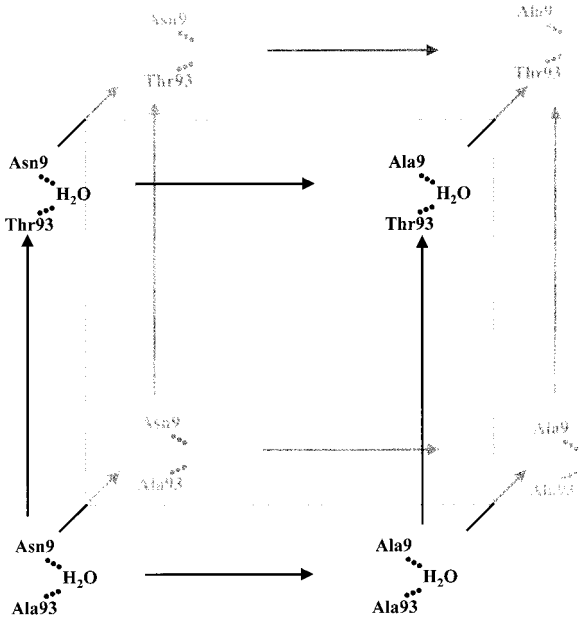

FIGURE 3: Double mutant cycle relating the changes in unfolding free energy ΔG, unfolding enthalpy ΔH and temperature-dependent entropy term $T\Delta S$ in the hydration site involving WAT1, Asn9, and Thr93, e.g., $\Delta(\Delta G) = \Delta G$(wild-type) − ΔG(mutant). ΔG is defined for unfolding. Thus, positive $\Delta(\Delta G)$ values show that the mutant is less stable than wild-type protein. All values (kcal/mol) are calculated at pH 7 and 50.2 °C.

In the present study, we removed the side chains of Asn9 and Thr93 of RNase T1 separately and then together by site-directed mutagenesis. Each residue is located at an opposite side of the hydration site under investigation (Figure 1a). We analyzed the conformational stabilities of all proteins by urea unfolding and differential scanning calorimetry and constructed a double mutant cycle from the corresponding results (Figure 3). The change of free energy for each side of the thermodynamic cycle was calculated [$\Delta(\Delta G)$]. By taking the difference between parallel sides of the cycle, we determined the difference in free energy between mutating one residue in the presence or absence of the other residue. This coupling free energy [$\Delta\Delta(\Delta G)$] of the thermodynamic cycle measures the strength of the mutual interactions between Asn9 and Thr93 (*27*). Because Asn9 and Thr93 interact through a single water molecule (WAT1) that is intercalated between their side chains, the coupling term of the cycle measures the strength of this water-mediated protein−protein interaction. Indeed, if the mutations do not cause structural rearrangements, the intramolecular interactions of Asn9 and Thr93 with the rest of the protein cancel out (*22*). To validate this point, we determined all relevant structures by X-ray crystallography.

Structural Validation of the Double-Mutant Cycle. For the present experimental approach to be valid, a functional group has to be removed without disturbing the structure of the protein either globally or locally. To verify this condition, it is necessary to determine the three-dimensional structures of the parent protein and the relevant point mutants. Wild-type RNase T1 and the mutants Asn9Ala, Thr93Ala, and Thr93Ala/Asn9Ala crystallize isomorphous in a crystal form that contains four RNase T1 molecules in its asymmetric unit, making it possible to separate differences caused by mutations from differences due to crystal lattice interactions. The quality of the different X-ray structures is given in Table 1. For each protein, there are a few loop structures that differ among the different molecules in the asymmetric unit. All these loops are involved in crystal packing and are located far away from the hydration site. These structural changes are therefore irrelevant for the present study. Crystallographically equivalent molecules (i.e., with respect to there position within the asymmetric unit) of wild-type RNase T1 and the mutants are identical within coordinate error. After superposition of the mutant structures onto the wild-type coordinates, the pairwise rms deviation for all backbone atoms varies between 0.08 and 0.17 Å. We observed no changes in backbone or side-chain conformations that can be ascribed as being a structural consequence of the introduced mutations.

Table 2: Interatomic Distances (Å) between WAT1 and the Surrounding O and N Atoms

	wild-type[a]	Asn9Ala[a]	Thr93Ala[a]	Asn9Ala/ Thr93Ala[a]
Cys6(O)···WAT1	3.0 ± 0.1	2.9 ± 0.1	3.1 ± 0.1	2.8 ± 0.1
Thr93(Oγ1)···WAT1	2.7 ± 0.1	2.7 ± 0.1		
Asp76(Oγ1)···WAT1	2.8 ± 0.1	2.8 ± 0.1	2.9 ± 0.2	2.8 ± 0.1
Thr91(Oγ1)···WAT1	3.4 ± 0.1	3.4 ± 0.1	3.6 ± 0.1	3.7 ± 0.1
Asn9(Nγ2)···WAT1	3.5 ± 0.1		3.2 ± 0.1	

[a] Average value calculated from four molecules in one asymmetric unit.

Figure 1 depicts the X-ray structures of the hydration site in wild-type RNase T1, the Asn9Ala and Thr93Ala single mutants, and the corresponding double mutant. Relevant interatomic distances and angles involving WAT1 are given in Tables 2 and 3. Neither the Asn9Ala and Thr93Ala single mutations nor the corresponding double mutation do perturb the local structure of the protein. WAT1 is conserved at a fixed position in the 16 independently refined molecules. The overall geometry of the hydration site is invariant to the side-chain deletions. Tables 2 and 3 show that the interatomic distances and the Y···O(W)···Y angles are within experimental error identical whether the side chains of Asn9 and Thr93 are deleted separately or together. As we do not observe any significant structural rearrangements, neither in the Asn9Ala and Thr93Ala single mutants nor in the corresponding double mutant, we conclude that the intramolecular interactions of Asn9 and Thr93 with the rest of the protein cancel out in the double mutant cycle presented in Figure 3. The coupling energy of this cycle therefore measures the strength of the WAT1 mediated interaction between Asn9 and Thr93.

Contributions of Asn9 and Thr93 to the Conformational Stability Are Additive. We used differential scanning calorimetry (DSC) and urea-induced unfolding to analyze the thermodynamic cycle involving Asn9 and Thr93 in order to distinguish an additive or cooperative contribution of both residues to the conformational stability of RNase T1. Table 4 lists the conformational stabilities of wild-type RNase T1, the Asn9Ala and Thr93Ala single mutants, and the corresponding double mutant as determined by urea-induced unfolding at pH 7 and 15, 25, and 35 °C. Unfolding of RNase T1 follows a two-state transition, and the folding process can be considered to be reversible (*28*); the free energy $\Delta G(H_2O)$ was determined by using linear extrapolation of ΔG toward zero concentration of denaturant according to Pace (*19*). To compare the free energies of unfolding of

Table 3: Analysis of All the Y···O(W)···Y Angles (α) of the Hydration Site

Y···O(W)···Y			α (deg)			
Y	O(W)	Y	wild-type[a]	Asn9Ala[a]	Thr93Ala[a]	Asn9Ala/Thr93Ala[a]
Asn9(Nδ2)	−WAT1−	Thr91(Oγ1)	135.5 ± 3.7		137.0 ± 6.0	
Asn9(Nδ2)	−WAT1−	Asp76(Oδ1)	84.0 ± 3.0		90.3 ± 4.5	
Asn9(Nδ2)	−WAT1−	Thr93(Oγ1)	151.9 ± 12.4			
Asn9(Nδ2)	−WAT1−	Cys6(O)	79.9 ± 3.7		81.8 ± 5.2	
Cys6(O)	−WAT1−	Asp76(Oδ1)	97.3 ± 1.4	104.5 ± 2.3	94.2 ± 6.0	104.4 ± 4.2
Cys6(O)	−WAT1−	Thr91(Oγ1)	102.7 ± 2.2	102.1 ± 1.6	94.7 ± 3.5	97.2 ± 3.6
Cys6(O)	−WAT1−	Thr93(Oγ1)	119.9 ± 18.6	123.9 ± 2.6		
Asp76(Oδ1)	−WAT1−	Thr91(Oγ1)	51.6 ± 1.7	50.0 ± 1.4	47.0 ± 1.7	46.6 ± 2.1
Asp76(Oδ1)	−WAT1−	Thr93(Oγ1)	111.5 ± 10.1	103.0 ± 2.7		
Thr91(Oγ1)	−WAT1−	Thr93(Oγ1)	61.5 ± 9.4	63.1 ± 2.3		

[a] Average value calculated from four molecules in one asymmetric unit. [b] Closest donor/acceptor sites are marked in bold characters.

Table 4: Conformational Stability at Different Temperatures Determined from Urea Unfolding Experiments

	15 °C		25 °C		35 °C	
protein	$urea_{1/2}$[a] (M)	$\Delta G(H_2O)$[b] (kcal/mol)	$urea_{1/2}$[a] (M)	$\Delta G(H_2O)$[b] (kcal/mol)	$urea_{1/2}$[a] (M)	$\Delta G(H_2O)$[b] (kcal/mol)
wild-type	6.14 ± 0.13	7.66 ± 0.21	4.97 ± 0.03	6.20 ± 0.12	3.34 ± 0.06	4.17 ± 0.10
Asn9Ala	5.47 ± 0.03	6.82 ± 0.12	4.36 ± 0.08	5.44 ± 0.14	2.87 ± 0.04	3.58 ± 0.08
Thr93Ala	5.45 ± 0.09	6.80 ± 0.16	4.41 ± 0.05	5.50 ± 0.12	2.86 ± 0.05	3.57 ± 0.09
Asn9Ala/Thr93Ala	4.93 ± 0.05	6.15 ± 0.12	3.99 ± 0.07	4.98 ± 0.12	2.17 ± 0.01	2.71 ± 0.05

[a] Midpoint of unfolding, urea concentration at which the fraction of unfolded protein equals $^1/_2$. [b] The free energies of unfolding have been extrapolated to 0 M urea using $\Delta G(H_2O) = m^* urea_{1/2}$. An average m value (1.247 kcal/mol M ± 0.025) was calculated from all measurements at 25 °C, pH 7.0.

Table 5: Thermodynamic Parameters at Different pHs Determined from DSC Measurements

	pH 5		pH 7		pH 10	
protein	T_{trs} (°C)	ΔH_{trs} (kcal/mol)	T_{trs} (°C)	ΔH_{trs} (kcal/mol)	T_{trs} (°C)	ΔH_{trs} (kcal/mol)
wild-type	60.3 ±0.2	95.2 ± 0.6	52.5 ±0.2	90.2 ± 0.6	43.0 ±0.2	74.2 ± 0.6
Asn9Ala	58.4 ±0.2	99.5 ± 0.6	50.3 ±0.2	92.0 ± 0.6	40.2 ±0.2	70.7 ± 0.6
Thr93Ala	58.5 ±0.2	93.1 ± 0.6	50.6 ±0.2	87.0 ± 0.6	41.0 ±0.2	73.1 ± 0.6
Asn9Ala/Thr93Ala	56.5 ±0.2	91.4 ± 0.6	47.8 ±0.2	84.9 ± 0.6	39.1 ±0.2	71.4 ± 0.6

different proteins at different temperatures more accurately, we made the validated assumptions that the *m* value changes between wild-type and mutants are minor (*29*, *30*) and that the *m* value does not depend on temperature (*31*−*33*). We used an invariable *m* value equal to the average of a large set of experimental values measured for wild-type RNase T1 and relevant mutants at 25 °C.

To characterize the proteins in question more reliably and comprehensively, the urea-unfolding studies were complemented by calorimetric measurements at pH 5, 7, and 10 (Table 5). For each protein sample, two consecutive scans were carried out. The second scan showed no significant difference compared to the first scan, indicating a reversible folding process. A ratio of the van't Hoff enthalpy ΔH_{vH} to the calorimetric enthalpy ΔH_{trs} of one is a necessary criterion for a two-state transition. For all our measurements, this ratio was close to one (data not shown), which is in good agreement with the results of other authors (*31*, *34*, *35*). According to the reversible two-state equilibration, DSC can be used to measure the thermodynamic parameters of unfolding of these proteins.

For wild-type RNase T1 and the mutants, we plotted the calorimetric determined transition free enthalpy ΔH_{trs} in dependence of the transition temperature T_{trs} according to the Kirchhoff relation (Figure 4). All data relate linearly with a correlation factor of 0.96, indicating that the change in heat capacity ΔC_p does not depend on temperature in the regarded temperature range. We therefore used throughout our discussion a constant ΔC_p value equal to the slope of this linear curve $\Delta C_p = 1273 \pm 114$ cal (mol K)$^{-1}$.

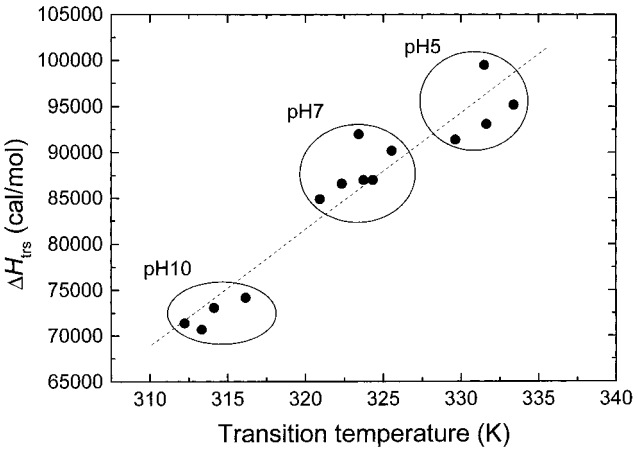

FIGURE 4: Plot of ΔH_{trs} of RNase T1 wild-type and all relevant mutants versus the corresponding transition temperature T_{trs} measured at different pHs (wild-type RnaseT1, magenta; Asn9Ala, green; Thr93Ala, blue; Asn9Ala/Thr93Ala, red). The slope of the linear extrapolation gives the change in heat capacity $\Delta C_p = 1273 \pm 114$ cal (mol K)$^{-1}$ according to the Kirchhoff relation (2). At pH 7, two additional mutants (Thr93Val, black; Thr93Gln; cyan) were included.

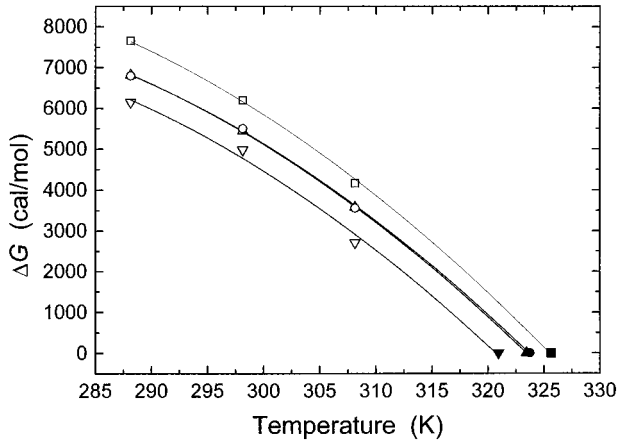

FIGURE 5: Plot of the free energy of unfolding ΔG versus temperature. The data points indicate the experimental values ($\Delta G_{measured}$) from DSC (filled symbols) and urea unfolding (open symbols). The lines are resulting from a nonlinear least-squares fit according to eq 1 (ΔG_{fit}) for wild-type RnaseT1 (magenta), Asn9Ala (green), Thr93Ala (blue), and Asn9Ala/Thr93Ala (red).

The modified Gibbs−Helmholtz equation (*1*) can be used to relate the free energies of unfolding determined from urea unfolding to those from DSC measurements. Figure 5 shows the experimental $\Delta G(H_2O)$ values from wild-type, Asn9Ala, Thr93Ala, and the double mutant obtained by the two different methods in function of temperature and the best fit curves to these data according to eq 1 using the constant ΔC_p value. The best fit parameters (data not shown) of the curves deviate less than 7% from the experimental DSC parameters. We conclude from this analysis that the free energies of unfolding determined from two independent methods confirm each other. The fitted curves provide us with reliable data over a broad temperature range for each mutant.

We calculated the free-energy contribution of the interactions of Asn9 and Thr93 through WAT1 to the conformational stability of RNase T1 by analyzing the thermodynamic cycle shown in Figure 3. Because the entropic and the enthalpic contributions may change with temperature, we calculated the coupling free energy of unfolding over a broad temperature range from the best-fit curves of Figure 5. Within the temperature range from 15 to 55 °C, the coupling free energies are small and do not exceed the absolute value of 300 cal/mol. We conclude from this approach that there is no free-energy coupling between Asn9 and Thr93 in the relevant temperature range.

Thermodynamics of the Water-Mediated Mutual Interactions between Asn9 and Thr93. The coupling energy obtained from a double mutant cycle measures the mutual interaction energy between the two residues under investigation because the interactions of each residue with the rest of the protein cancel out (see above). Because the conformational stability of a protein is defined as the free-energy difference between its folded and unfolded state, the coupling energy determined in our study compares the free energy of the mutual interactions between Asn9 and Asn93 in the folded state and the unfolded state of the protein. The observation that Asn9 and Thr93 contribute additively to the conformational stability of RNase T1 indicates that the mutual interaction energy between Asn9 and Thr93 is similar in the folded and the unfolded state (Figure 6). In the folded state, this

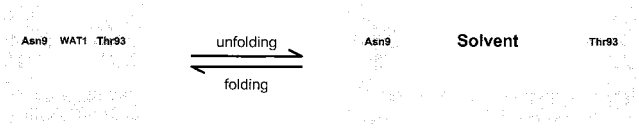

FIGURE 6: Illustration of the water mediated interactions between residue Asn9 and Thr93 in the folded and unfolded state.

interaction involves the intercalated WAT1 molecule. In the unfolded state, Asn9 and Thr93 are separated by bulk solvent because they are located at opposite ends of the linear sequence of RNase T1. There is the formal possibility that the two disulfide bridges (2−10, 6−103) that cross-link the unfolded state of RNase T1 force Asn9 and Thr93 to interact in the unfolded state (*38*). Because nine residues separate Thr93 from Cys103, we rule out such a contact. Taken together, we conclude that the free energy of the WAT1-mediated protein−protein interaction in the folded state is very similar to the solvent-mediated protein−protein interaction in the unfolded state. In other words, the WAT1-mediated mutual interaction between Asn9 and Thr93 does not contribute to the conformational stability of the folded state, as compared to the unfolded state.

There is ample experimental evidence that the entropy and the enthalpy changes compensate each other to a high degree in a variety of processes including solvation of ions and nonelectrolytes, chemical reactions, ionizations of weak electrolytes, ligand binding, and protein folding and stability (*39*). Although Asn9 and Thr93 contribute additively to the conformational stability of RNase T1, their mutual interaction enthalpy and entropy may change significantly upon folding.

Aiming to address this question, we investigated the enthalpic and entropic contribution of the interactions between Asn9 and Thr93 to the conformational stability. For this purpose, we calculated the enthalpic term ΔH and entropic term $T\Delta S$ for wild-type RNase T1, the Asn9Ala and Thr93Ala single mutants, and the corresponding double mutant according to eqs 2 and 3 at 50.2 °C and analyzed their interdependence with a thermodynamic cycle (Figure 3). In this model, we used the best-fit parameters of ΔH_{trs} and T_{trs} from the curves shown in Figure 5, based on DSC and urea unfolding data over a broad temperature range. A temperature of 50.2 °C is the average melting temperature of the investigated proteins at pH 7.0. The differences between this average and the actual melting temperature of each mutant are small. Therefore, extrapolations are limited to a small temperature interval. As a result, the errors on ΔH and $T\Delta S$ are kept to a minimum upon extrapolation.

According to this model, the enthalpic contribution of the mutual interaction between Asn9 and Thr93 involving WAT1 to the conformational stability [$\Delta\Delta(\Delta H) = 3.6 \pm 2.5$ kcal mol^{-1}] appears to be significant at 50.2 °C. This suggests that the mutual interaction enthalpy between both residues is stronger in the folded state as compared to the unfolded state. In the folded state, this interaction is mediated by WAT1. In the unfolded state, this interaction is mediated by bulk solvent (Figure 6). The interaction entropy between Asn9 and Thr93 [$T\Delta\Delta(\Delta S) = 3.9 \pm 2.6$ K kcal mol^{-1}] is smaller in the folded state as compared to the unfolded state. It thus appears that the Asn9···WAT1···Thr93 interaction in the folded state is enthalpically more stable but entropically

disfavored as compared to Asn9···solvent···Thr93 in the unfolded state.

We would like to end our discussion with a small note of precaution. Although we believe that this new experimental approach to investigate protein hydration is valid and valuable, we intend to investigate more hydration sites by double mutant cycles to further substantiate our conclusions, especially on enthalpy−entropy compensation. First, the values for $\Delta\Delta(\Delta H)$ and $\Delta\Delta(\Delta S)$ are just slightly greater than the standard deviation, which means that the probability of the true value of $\Delta\Delta(\Delta H)$ being outside the range 1.1−6.1 kcal/mol is 32% (assuming no systematic errors). As indicated by a referee, the apparent enthalphy−entropy compensation may also come from the model since ΔH and ΔS are not measured independently but calculated using eqs 2 and 3. Assuming temperature-independent ΔC_p and $\Delta T = (T_{trs} - T) \ll T_{trs}$, one can recombine eqs 2 and 3 to

$$\Delta H(T) - T\Delta S(T) = \Delta H_{trs}(\Delta T/T_{trs}) \qquad (4)$$

The compensation may thus be a feature of the model, not the system. In an early review of the subject (*39*), this kind of apparent compensation was called "accidental".

CONCLUSIONS

In the present paper, we describe a new experimental approach to study solvent mediated protein−protein interactions. The method rests on evaluating the interdependence of the contribution of two side chains to the conformational stability of a protein with a double mutant cycle. Both side chains have to be involved in the "solvation" of the same water molecule. We applied this technique to Asn9 and Thr93, two residues that are part of a conserved hydration site in RNase T1. We conclude that the free energy of the Asn9···WAT1···Thr93 interaction in the folded state is very similar to that of to Asn9···Solvent···Thr93 interaction in the unfolded state. It appears that sequestering WAT1 in the folded structure of RNase T1 reduces the WAT1 mediated interaction entropy between Asn9 and Thr93. This loss of entropy is compensated for by more favorable enthalpic interactions among Asn9, WAT1 and Thr93 in the folded state as compared to the interactions of Asn9 and Thr93 mediated by bulk solvent in the unfolded state.

ACKNOWLEDGMENT

We would like to thank the Vlaams Interuniversitair Instituut voor Biotechnologie and the Fonds voor Wetenschappelijk Onderzoek Vlaanderen for financial support. We wish to thank Elke Brosens for technical assistance and the referees for valuable comments. R. Loris is research associate of the Fonds voor Wetenschappelijk Onderzoek Vlaanderen.

REFERENCES

1. Sreenivasan, U., and Axelsen, P. H. (1992) Buried water in homologous serine proteases. *Biochemistry 31*, 12785−12791.
2. Loris, R., Langhorst, U., De Vos, S., Decanniere, K., Bouckaert, J., Maes, D., Transue, T. R., and Steyaert, J. (1999) Conserved water molecules in a large family of microbial ribonucleases. *Proteins 36*, 117−134.
3. Loris, R., Stas, P. P., and Wyns, L. (1994) Conserved waters in legume lectin crystal structures. The importance of bound water for the sequence-structure relationship within the legume lectin family. *J. Biol. Chem. 269*, 26722−26733.
4. Levitt, M., and Park, B. H. (1993) Water: now you see it, now you do not. *Structure 1*, 223−226.
5. Otting, G., Liepinsh, E., and Wuthrich, K. (1991) Protein hydration in aqueous solution. *Science 254*, 974−980.
6. Denisov, V. P., Halle, B., Peters, J., and Horlein, H. D. (1995) Residence times of the buried water molecules in bovine pancreatic trypsin inhibitor and its G36S mutant. *Biochemistry 34*, 9046−9051.
7. Williams, M. A., Goodfellow, J. M., and Thornton, J. M. (1994) Buried waters and internal cavities in monomeric proteins. *Protein Sci. 3*, 1224−1235.
8. Baker, E. N., and Hubbard, R. E. (1984) Hydrogen bonding in globular proteins. *Prog. Biophys. Mol. Biol. 44*, 97−179.
9. Langhorst, U., Loris, R., Denisov, V. P., Doumen, J., Roose, P., Maes, D., Halle, B., and Steyaert, J. (1999) Dissection of the structural and functional role of a conserved hydration site in RNase T1. *Protein Sci. 8*, 722−730.
10. Steyaert, J., Hallenga, K., Wyns, L., and Stanssens, P. (1990) Histidine-40 of ribonuclease T1 acts as base catalyst when the true catalytic base, glutamic acid-58, is replaced by alanine. *Biochemistry 29*, 9064−9072.
11. Chen, B., and Przybyla, A. E. (1994) An efficient site-directed mutagenesis method based on PCR. *Biotechniques 17*, 657−659.
12. Mayr, L. M., and Schmid, F. X. (1993) A purification method for labile variants of ribonuclease T1. *Protein Expression Purif. 4*, 52−58.
13. Otwinowski, Z., and Minor, W. (1997) in *Methods in Enzymology* (Carter, C. W., and Sweet, R. M., Eds.) pp 307−326, Academic Press, New York.
14. Collaborative Computational Project, Number 4 (1994) The CCP4 suite: Programs for Crystallography. *Acta Crystallogr., Sect. D 50*, 760−763.
15. Navaza, J. (1994) AMoRe: An automated package for molecular replacement. *Acta Crystallogr., Sect. A 50*, 157−163.
16. Zegers, I., Haikal, A. F., Palmer, R., and Wyns, L. (1994) Crystal structure of RNase T1 with 3′-guanylic acid and guanosine. *J. Biol. Chem. 269*, 127−133.
17. Brünger, A. T. (1992). X-PLOR: A system for crystallography and NMR. Yale University, New Haven, Connecticut.
18. Laskowski, R. A., MacArthur, M. W., Moss, D. S., and Thornton, J. M. (1993) Procheck: a program to check the stereochemical quality of protein structures, *J. Appl. Crystallgr. 26*, 283−291.
19. Pace, C. N. (1986) Determination and analysis of urea and guanidine hydrochloride denaturation curves. *Methods Enzymol. 131*, 266−280.
20. Shirley, B. A., and Laurents, D. V. (1990) Purification of recombinant ribonuclease T1 expressed in *Escherichia coli*. *J. Biochem. Biophys. Methods 20*, 181−188.
21. Santoro, M. M., and Bolen, D. W. (1988) Unfolding free energy changes determined by the linear extrapolation method. 1. Unfolding of phenylmethanesulfonyl alpha-chymotrypsin using different denaturants. *Biochemistry 27*, 8063−8068.
22. Horovitz, A. (1996) Double-mutant cycles: a powerful tool for analyzing protein structure and function. *Folding Des. 1*, 121−126.
23. Wells, J. A. (1990) Additivity of mutational effects in proteins. *Biochemistry 29*, 8509−8517.
24. Tilton, R. F. J., Singh, U. C., Weiner, S. J., Connolly, M. L., Kuntz, I. D. J., Kollman, P. A., Max, N., and Case, D. A. (1986) Computational studies of the interaction of myoglobin and xenon. *J. Mol. Biol. 192*, 443−456.
25. Baldwin, E., Baase, W. A., Zhang, X., Feher, V., and Matthews, B. W. (1998) Generation of ligand binding sites in T4 lysozyme by deficiency-creating substitutions. *J. Mol. Biol. 277*, 467−485.
26. Prange, T., Schiltz, M., Pernot, L., Colloc'h, N., Longhi, S., Bourguet, W., and Fourme, R. (1998) Exploring hydrophobic sites in proteins with xenon or krypton. *Proteins 30*, 61−73.
27. Horovitz, A., and Fersht, A. R. (1990) Strategy for analysing the cooperativity of intramolecular interactions in peptides and proteins. *J. Mol. Biol. 214*, 613−617.

28. Thomson, J. A., Shirley, B. A., Grimsley, G. R., and Pace, C. N. (1989) Conformational stability and mechanism of folding of ribonuclease T1. *J. Biol. Chem. 264*, 11614−11620.
29. Shirley, B. A., Stanssens, P., Hahn, U., and Pace, C. N. (1992) Contribution of hydrogen bonding to the conformational stability of ribonuclease T1. *Biochemistry 31*, 725−732.
30. Myers, J. K., Pace, C. N., and Scholtz, J. M. (1995) Denaturant m values and heat capacity changes: relation to changes in accessible surface areas of protein unfolding. *Protein Sci. 4*, 2138−2148.
31. Hu, C. Q., Sturtevant, J. M., Thomson, J. A., Erickson, R. E., and Pace, C. N. (1992) Thermodynamics of ribonuclease T1 denaturation. *Biochemistry 31*, 4876−4882.
32. Agashe, V. R., and Udgaonkar, J. B. (1995) Thermodynamics of denaturation of barstar: evidence for cold denaturation and evaluation of the interaction with guanidine hydrochloride. *Biochemistry 34*, 3286−3299.
33. Backmann, J., Schäfer, G., Wyns, L., and Bönisch, H. (1998) Thermodynamics and kinetics of unfolding of the thermostable trimeric adenylate kinase from the A*rchaeon sulfolobus acidocaldarius*, *J. Mol. Biol. 284*, 817−833.
34. Schubert, W. D., Schluckebier, G., Backmann, J., Granzin, J., Kisker, C., Choe, H. W., Hahn, U., Pfeil, W., and Saenger, W. (1994) X-ray crystallographic and calorimetric studies of the effects of the mutation Trp59→Tyr in ribonuclease T1. *Eur. J. Biochem. 220*, 527−534.
35. Yu, Y., Makhatadze, G. I., Pace, C. N., and Privalov, P. L. (1994) Energetics of ribonuclease T1 structure. *Biochemistry 33*, 3312−3319.
36. Sandberg, W. S., and Terwilliger, T. C. (1993) Engineering multiple properties of a protein by combinatorial mutagenesis, *Proc. Natl. Acad. Sci. U.S.A. 90*, 8367−8371.
37. Dill, K. A. (1997) Additivity principles in biochemistry. *J. Biol. Chem. 272*, 701−704.
38. Pace, C. N., Grimsley, G. R., Thomson, J. A., and Barnett, B. J. (1988) Conformational stability and activity of ribonuclease T1 with zero, one, and two intact disulfide bonds. *J. Biol. Chem. 263*, 11820−11825.
39. Lumry, R., and Rajender, S. (1970) Enthalpy−entropy compensation phenomena in water solutions of proteins and small molecules: a ubiquitous property of water. *Biopolymers 9*, 1125−1227.

BI992131M